

# Halogen Bonding in *N*-Alkyl-3-halogenopyridinium Salts

Luka Fotović  and Vladimir Stilinović \* 

Department of Chemistry, Faculty of Science, University of Zagreb, Horvatovac 102a, HR-10002 Zagreb, Croatia; lfotovic@chem.pmf.hr

\* Correspondence: vstilinovic@chem.pmf.hr; Tel.: +385-1-4606-371

**Abstract:** We performed a structural study of *N*-alkylated halogenopyridinium cations to examine whether choice of the *N*-substituent has any considerable effect on the halogen bonding capability of the cations. For that purpose, we prepared a series of *N*-ethyl-3-halopyridinium iodides and compared them with their *N*-methyl-3-halopyridinium analogues. Structural analysis revealed that *N*-ethylated halogenopyridinium cations form slightly shorter C–X···I<sup>−</sup> halogen bonds with iodide anion. We have also attempted synthesis of ditopic symmetric bis-(3-iodopyridinium) dication. Although successful in only one case, the syntheses have afforded two novel ditopic asymmetric monocations with an iodine atom bonded to the pyridine ring and another on the aliphatic *N*-substituent. Here, the C–I···I<sup>−</sup> halogen bond lengths involving pyridine iodine atom were notably shorter than those involving an aliphatic iodine atom as a halogen bond donor. This trend in halogen bond lengths is in line with the charge distribution on the Hirshfeld surfaces of the cations—the positive charge is predominantly located in the pyridine ring making the pyridine iodine atom  $\sigma$ -hole more positive than the one on the alkyl chain.

**Keywords:** pyridinium cations; halogen bond; halogenide anions



**Citation:** Fotović, L.; Stilinović, V. Halogen Bonding in *N*-Alkyl-3-halogenopyridinium Salts. *Crystals* **2021**, *11*, 1240. <https://doi.org/10.3390/cryst11101240>

Academic Editors: Sergiy Rosokha and Atash V. Gurbanov

Received: 29 September 2021  
Accepted: 12 October 2021  
Published: 14 October 2021

**Publisher's Note:** MDPI stays neutral with regard to jurisdictional claims in published maps and institutional affiliations.



**Copyright:** © 2021 by the authors. Licensee MDPI, Basel, Switzerland. This article is an open access article distributed under the terms and conditions of the Creative Commons Attribution (CC BY) license (<https://creativecommons.org/licenses/by/4.0/>).

## 1. Introduction

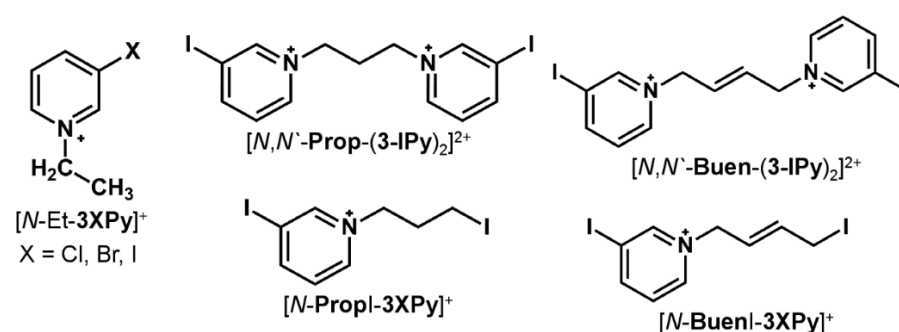
A halogen bond [1–5], an attractive  $\sigma$ -hole [6–8] interaction between a halogen atom (Lewis acid) and a Lewis base, is a well-established tool of crystal engineering and supramolecular chemistry [9–12]. To date, various Lewis bases (neutral molecules or charged species) have been employed as halogen bond acceptors in constructing halogen-bonded supramolecular assemblies. These have most commonly been organic [13,14] and metal-organic [15] molecules containing electron-rich nitrogen [16–26] and oxygen atoms [27–41], as well as inorganic anions such as halogenides [42–54]. The most commonly used halogen bond donors have traditionally been neutral organic molecules where a halogen atom is bonded to electron-withdrawing molecular residues. Fluorine atoms [55–60], nitro and cyano groups [61–65], or C–C triple bond [16,66–68], exhibit an electron withdrawing effect on the halogen atom and consequently increase the positive electrostatic potential (ESP) of the  $\sigma$ -hole of the halogen atom. The same effect can be archived if the halogen atom is bonded to a more electronegative heteroatom such as nitrogen in *N*-halogenoimides [69–76] or oxygen in organic hypoiodites [77].

There is an alternative approach to making a reliable halogen bond donor by placing a halogen atom on a positively charged species. To date, a number of halogenoimidazolium and halogenopyridinium cations employed as halogen bond donors in salts with organic [78,79] and inorganic [13,25,44–54,80–91] counterions have been published. Halogenopyridinium cations have been studied as anion receptors [92–96], catalysts in halogenide abstraction [97], colour tuning [98,99] and as counterions for tuning conductivity and magnetic properties in supramolecular conductors [100–103].

Generally, *N*-methylation of halogenopyridines (iodopyridines in particular) greatly increases the ESP of the  $\sigma$ -hole of the halogen atom, rendering them formidable halogen bond donors. This is also evident from the structural data, which show that iodopyridinium

cations tend to form quite short halogen bonds with both neutral and anionic halogen bond acceptors, such as halogenide anions [104].

Herein, we report a structural study of a series of halogenides of *N*-alkylated 3-halogenopyridinium cations with *N*-substituents other than methyl group. In the first place, we prepared a series of *N*-ethyl-3-halopyridinium (chloro, bromo and iodo) iodides, in order to compare them with the *N*-methyl-3-halopyridinium analogues to examine whether the increased *N*-substituent has any observable effect on the halogen bonding capability of the cations. In addition, we have attempted preparation of dicationic species comprising a pair of 3-iodopyridinium rings separated by an aliphatic linker, which might act as ditopic cationic halogen bond donors (Scheme 1).



**Scheme 1.** Cationic halogen bond donors examined in this study.

## 2. Materials and Methods

All the solvents used (ethanol, acetone, dichloromethane) were procured from Sigma-Aldrich Chemie GmbH, Taufkirchen, Germany. Ethyl iodide (EtI) and 3-chloropyridine (**3-ClPy**) were procured from Acros Organics, Fisher Scientific UK Ltd., Leicestershire, United Kingdom. 3-bromopyridine (**3-BrPy**), 3-iodopyridine (**3-IPy**), 4-iodopyridine (**4-IPy**), 1,3-diiodopropane (**PropI<sub>2</sub>**) and 1,4-dibromobuta-2-ene (**BuenBr<sub>2</sub>**) were procured from Apollo Scientific Ltd., Cheshire, United Kingdom. All reagents, as well as the organic solvents, were used without additional purification.

### 2.1. Solution and Single Crystal Synthesis of Cocrystals

*N*-ethyl-3-chloropyridinium iodide [**N-Et-3-ClPy**]I was obtained by dissolving halogenopyridine (1 mmol) in hot acetone and adding ethyl iodide in excess (ca 1.2 mmol) whereupon the solutions were left to cool and evaporate. Yellow crystals suitable for single-crystal X-ray diffraction experiments appeared in one day. Yield: 213 mg (79%).

*N*-ethyl-3-bromopyridinium iodide [**N-Et-3-BrPy**]I was obtained by dissolving halogenopyridine (1 mmol) in hot dichloromethane and adding ethyl iodide in excess (ca 1.2 mmol) whereupon the solution was left to cool and evaporate. Brown crystals suitable for single-crystal X-ray diffraction experiments appeared in three days. Yield: 183 mg (58%).

*N*-ethyl-3-iodopyridinium iodide [**N-Et-3-IPy**]I was obtained by dissolving halogenopyridine (1 mmol) in hot dichloromethane and adding ethyl iodide in excess (ca 1.2 mmol) whereupon the solution was left to cool and evaporate. Yellow crystals suitable for single-crystal X-ray diffraction experiments appeared in three days. Yield: 297 mg (82%).

*N*-(2-oxopropyl)-3-bromopyridinium iodide ([**N-Ace-3-BrPy**]I) was obtained by dissolving 3-bromopyridine (1 mmol) in hot acetone and adding ethyl iodide in excess (ca 1.2 mmol) whereupon the solution was left to cool and evaporate. Mixture of brown crystals ([**N-Et-3-BrPy**]I and [**N-Ace-3-BrPy**]I) appeared in 12 h.

4-iodopyridinium hemihydroiodide ([**4-IPy**]<sub>2</sub>HI) was obtained by dissolving 4-iodopyridine (1 mmol) in mixture of hot acetone and dichloromethane (1:1; volume ratio) and adding ethyl iodide in excess (ca 1.2 mmol) whereupon the solution was left to cool and evaporate. Blue crystals suitable for single-crystal X-ray diffraction experiments appeared in one day.

*N*-(3-iodopropanyl)-3-iodopyridinium iodide ([*N*-IProp-3-IPy]I) was obtained by dissolving 3-iodopyridine (2 mmol) in hot acetone and adding 1,3-diiodopropane (1 mmol) whereupon the solution was left to cool and evaporate. Yellow powder appeared in three days, while yellow crystals suitable for single-crystal X-ray diffraction experiments appeared in ten days. Yield: 144 mg (29%).

(2*E*)-1,4-bis(pyridin-1-ium-1-yl)but-2-ene dibromide ([*N,N'*-Buen-(3-IPy)<sub>2</sub>]Br<sub>2</sub>) was obtained by dissolving 3-iodopyridine (2 mmol) in mixture of hot acetone and ethanol (1:1; volume ratio) and adding (*E*)-1,4-dibromobuta-2-ene (1 mmol) whereupon the solution was left to cool and evaporate. White microcrystalline product appeared in one day. Yield: 494 mg (79%).

*N*-((2*E*)-4-iodobuta-2-enyl)-3-iodopyridinium iodide ([*N*-IBuen-3-IPy]I) was obtained by dissolving [*N,N'*-Buen-(3-IPy)<sub>2</sub>]Br<sub>2</sub> (1 mmol) in deionized water (20 mL) and passing the solution through an anion exchange column. The ion-exchange resin (Dowex 21K chloride form, 16-30 mesh, Sigma-Aldrich Chemie GmbH, Taufkirchen, Germany) was regenerated with 50 mL aqueous solution of sodium hydroxide (*c* = 1 mol L<sup>-1</sup>). Hydroiodic acid (*c* = 1 mol L<sup>-1</sup>) was added dropwise in the obtained solution until neutralization. Yellow crystals suitable for single-crystal X-ray diffraction experiments appeared in three days. Yield: 57 mg (9%).

Single crystals (suitable for single crystal X-ray diffraction experiment) of [3-CIPyMe]I, [3-BrPyMe]I, [3-IPyMe]I, [*N*-Ace-3-BrPy]I, [4IPy]<sub>2</sub>HI, [*N*-IProp-3-IPy]I and [*N*-IBuen-3-IPy]I were obtained from the synthetic procedure, while single crystals of ([*N,N'*-Buen-(3-IPy)<sub>2</sub>]Br<sub>2</sub>) were prepared by crystalizing the initially obtained microcrystalline salt from mixture of ethanol and water (3:1; volume ratio).

FT-IR (ATR) spectra of prepared compounds are shown in Figures S21–S26 in Supplementary Materials.

## 2.2. Powder X-ray Diffraction Measurements

Powder X-ray diffraction experiments on the samples were performed on an Aeris X-ray diffractometer (Malvern Panalytical, Malvern Worcestershire, UK) with CuK $\alpha$ 1 ( $\lambda$  = 1.54056 Å) radiation. The scattered intensities were measured with a PIXcel-1D-Medipix3 detector. The angular range was from 5° to 40° (2 $\theta$ ) with a continuous step size of 0.02° and measuring a time of 0.5 s per step.

Data collection methods were created using the program package START XRDMP CREATOR (Malvern Panalytical, Malvern Worcestershire, UK) while the data were analysed using X'Pert HighScore Plus (Version 2.2, Malvern Panalytical, Malvern Worcestershire, UK) [105]. Comparison of measured and calculated PXRD patterns of the prepared compounds are shown in Figures S9–S14 in Supplementary Materials.

## 2.3. Single Crystal X-ray Diffraction Measurements

Single crystal X-ray diffraction experiments were performed using an Oxford Diffraction Xcalibur Kappa CCD X-ray diffractometer (Oxford Diffraction Ltd., Abingdon, UK) with graphite-monochromated MoK $\alpha$  ( $\lambda$  = 0.71073 Å) radiation. The data sets were collected using the  $\omega$ -scan mode over the 2 $\theta$ —range up to 54°. Programs CrysAlis PRO CCD and CrysAlis PRO RED were employed for data collection, cell refinement, and data reduction [106,107]. The structures were solved and refined using SHELXS (Version 2013, Göttingen, Germany), SHELXL programs (Version 2013, Göttingen, Germany), SHELXT programs (Version 2013, Göttingen, Germany), respectively [108,109]. The structural refinement was performed on  $F^2$  using all data. The hydrogen atoms were placed in calculated positions and treated as riding on their parent atoms (C–H = 0.93 Å and  $U_{\text{iso}}(\text{H}) = 1.2 U_{\text{eq}}(\text{C})$  for aromatic and methine hydrogen atoms; C–H = 0.96 Å and  $U_{\text{iso}}(\text{H}) = 1.5 U_{\text{eq}}(\text{C})$  for methyl hydrogen atoms, C–H = 0.97 Å and  $U_{\text{iso}}(\text{H}) = 1.2 U_{\text{eq}}(\text{C})$  for methylene hydrogen atoms). The position of the proton in [4-IPy $\cdots$ H $\cdots$ 4-IPy]<sup>+</sup> cation could not be reliably located from the electron difference map, and it was modelled as disordered over two positions on the nitrogen atoms of both 4-IPy molecules with

0.5 occupancy. All calculations were performed using the WinGX or Olex2 1.3-ac4 crystallographic suite of programs [110,111]. The figures were prepared using Mercury 2020.2.0 (CCDC, Cambridge, UK) [112]. Crystallographic data of the prepared compounds are shown in Table S2 in Supplementary Materials. ORTEP plots of the obtained compounds are shown in Figures S1–S8 in Supplementary Materials. CCDC No. 2109490–2109497, contain crystallographic data for this paper.

#### 2.4. Thermal Analysis

Differential scanning calorimetry (DSC) and thermogravimetric (TG) measurements were performed simultaneously on a Mettler-Toledo TGA/DSC 3+ module (Mettler Toledo, Greifensee, Switzerland). Samples were placed in alumina crucibles (40  $\mu$ L) and heated 25 to 300  $^{\circ}$ C, at a heating rate of 10  $^{\circ}$ C  $\text{min}^{-1}$  under nitrogen flow of 150  $\text{mL min}^{-1}$ .

Data collection and analysis were performed using the program package STARe Software (Version 15.00, Mettler Toledo, Greifensee, Switzerland) [113]. TG and DSC thermograms of the prepared compounds are shown in Figures S15–S20 in the Supplementary Materials.

#### 2.5. Calculations

All calculations were performed using CrystalExplorer software package [114]. Hirshfeld surfaces were generated with high resolution. Molecular electrostatic potentials were calculated at B3LYP-DGDZVP level of theory [115–118].

### 3. Results and Discussion

All three *meta*-halogenopyridines (chloro, bromo and iodo) were successfully *N*-ethylated using EtI, producing corresponding iodide salts. The crystal structure of [N-Et-3-ClPy]I comprises centrosymmetric cyclical [N-Et-3-ClPy]<sub>2</sub>I<sub>2</sub> tetramers in which [N-Et-3-ClPy]<sup>+</sup> cations and iodide anions are interconnected through C–H $\cdots$ I<sup>−</sup> hydrogen bonds ( $d(\text{C}3\cdots\text{I}1) = 3.901(6)$  Å,  $d(\text{C}4\cdots\text{I}1) = 3.876(6)$  Å) (Figure 1a). C–H $\cdots$ I<sup>−</sup> hydrogen bonds and anion- $\pi$  interactions,  $d(\text{C}5\cdots\text{I}1) = 3.729(7)$  Å). The tetramers are connected into a layer via C–H $\cdots$ I<sup>−</sup> hydrogen bonds ( $d(\text{C}1\cdots\text{I}1) = 3.866(6)$  Å), and the layers are then stacked on top of each other. Chlorine atoms do not participate in any significant supramolecular interactions. Analysing the electrostatic potential plotted on the Hirshfeld surface (Figure 1b), it has been found that ESP on the Hirshfeld surface in the  $\sigma$ -hole area (0.112 a.u.) is less positive than the mean ESP of chloropyridinium cation (0.148 a.u.). On the other hand, ESP on Hirshfeld surface near hydrogen atoms, which participate in supramolecular interactions, corresponds to the most positive regions of the [N-Et-3-ClPy]<sup>+</sup> cation (0.229 au).

Substitution of chlorine on the pyridine ring with bromine leads to a significant difference in the structural arrangement of the cations and anions. The main difference is the presence of a C–Br $\cdots$ I<sup>−</sup> halogen bond shorter by ca. 6% than the sum of the corresponding van der Waals radii ( $d(\text{Br}1\cdots\text{I}1) = 3.611(7)$  Å,  $\angle(\text{C}2\text{--}\text{Br}1\cdots\text{I}1) = 169.2(2)^{\circ}$ ). A methylene hydrogen atom of the ethyl group participates in a C–H $\cdots$ I<sup>−</sup> hydrogen bond with the iodide anion ( $d(\text{C}6\cdots\text{I}1) = 4.013(6)$  Å). This combination of halogen and hydrogen bonds connects bromopyridinium cations and iodide anions in helical chains extending along the crystallographic *b* axis. The iodide anions also participate in anion- $\pi$  contacts ( $d(\text{C}1\cdots\text{I}1) = 3.575(5)$  Å) with cations from the neighbouring chains, which leads to formation of layers perpendicular to the *c* axis in the structure of [N-Et-3-BrPy]I (Figure 2).

In the structure of [N-Et-3-Ipy]I the cations and the anions are also connected in chains (along the crystallographic *b* axis) with combinations of C–I $\cdots$ I<sup>−</sup> halogen bonds ( $d(\text{I}1\cdots\text{I}2) = 3.473(3)$  Å,  $\angle(\text{C}2\text{--}\text{I}1\cdots\text{I}2) = 178.25(7)^{\circ}$ ) shorter by ca. 12% than the sum of the corresponding van der Waals radii, and C–H $\cdots$ I<sup>−</sup> hydrogen bonds ( $d(\text{C}1\cdots\text{I}2) = 3.778(3)$  Å), but here the hydrogen bond is formed by an aromatic hydrogen atom in ortho position to the pyridine nitrogen. The chains are connected into layers via C–H $\cdots$ I<sup>−</sup> hydrogen bonds ( $d(\text{C}7\cdots\text{I}2) = 4.094(3)$  Å) with a methyl hydrogen atom (Figure 3).

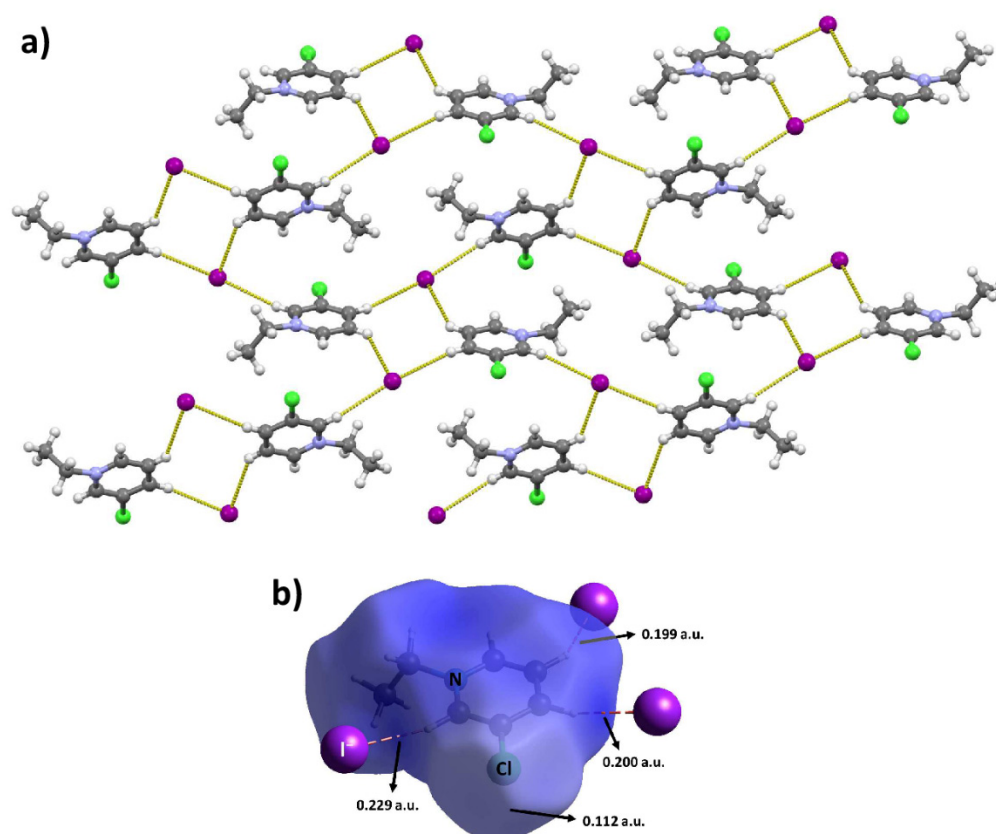


**Figure 1.** (a) Layers of  $[N\text{-Et-3-ClPy}]^+$  cations and iodide anions connected through  $\text{C-H}\cdots\text{I}^-$  hydrogen bonds in the structure of  $[N\text{-Et-3-ClPy}]\text{I}$ ; (b) Hirshfeld surface with mapped ESP (computed on B3LYP-DGDZVP level of theory) of the  $[N\text{-Et-3-ClPy}]^+$  cation and the contact iodide anions in  $[N\text{-Et-3-ClPy}]\text{I}$ .

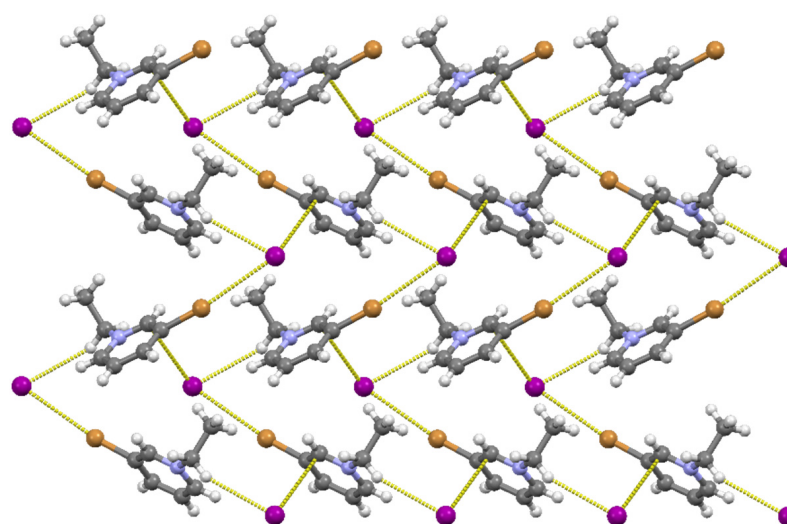


**Figure 2.**  $[N\text{-Et-3-BrPy}]^+$  cations and iodide anions connected into layers through  $\text{C-Br}\cdots\text{I}^-$  halogen bonds,  $\text{C-H}\cdots\text{I}^-$  hydrogen bonds and anion- $\pi$  contacts in the structure of  $[N\text{-Et-3-BrPy}]\text{I}$ .

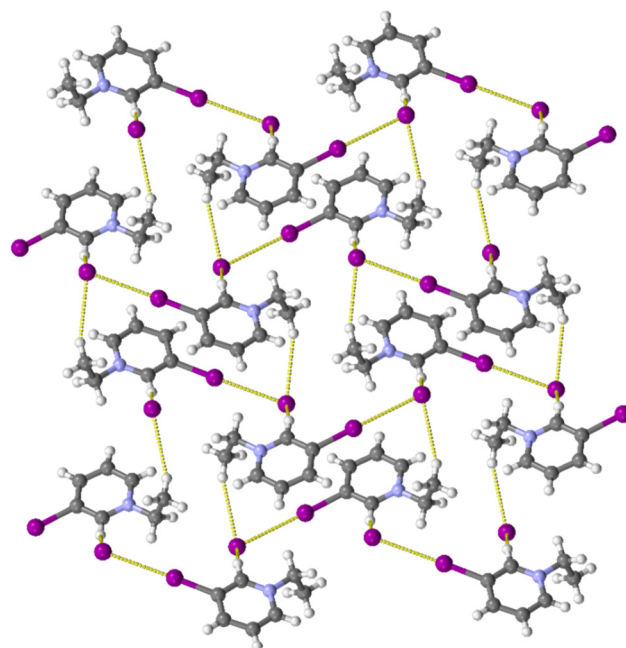


**Figure 3.**  $[N\text{-Et-3-IPy}]^+$  cations and iodide anions connected into layers through  $\text{C-I}\cdots\text{I}^-$  halogen bonds and  $\text{C-H}\cdots\text{I}^-$  hydrogen bonds in the structure of  $[N\text{-Et-3-IPy}]\text{I}$ .

The halogen bond strengths also reflect the thermal stability of the iodide salts of the *N*-ethylated 3-halogenopyridines. The inspection of the results of the thermal analysis (see DSC and TG thermograms in the ESI) revealed that all three compounds exhibit well-defined melting points, which are then followed by simultaneous decomposition and evaporation. Melting point temperatures increase from 110 °C for  $[N\text{-Et-3-ClPy}]\text{I}$  to 116 °C for  $[N\text{-Et-3-BrPy}]\text{I}$  and finally 127 °C for  $[N\text{-Et-3-IPy}]\text{I}$  showing a clear increase in the melting point temperature with the size of halogen bond donor atom and, therefore, the strength of the  $\text{C-X}\cdots\text{I}^-$  halogen bond.

If one is to compare halogen bonding in *N*-ethylated 3-halogenopyridinium iodides to those in *N*-methylated 3-halogenopyridinium iodides, one can see that in both series cations derived from 3-bromopyridine and 3-iodopyridine participate in  $\text{C-X}\cdots\text{I}^-$  halogen bonds. Conversely, in *N*-ethyl-3-chloropyridinium iodide, cations do not participate in halogen bonding, while in *N*-methyl-3-chloropyridinium iodide some of symmetrically independent cations participate in the  $\text{C-Cl}\cdots\text{I}^-$  halogen bonds with iodide anion, but these halogen bonds are longer than the sum of the corresponding van der Waals radii. When comparing the lengths of the halogen bonds in the two series of iodides, both the  $\text{C-Br}\cdots\text{I}^-$  and the  $\text{C-I}\cdots\text{I}^-$  halogen bonds are shorter in the *N*-ethylated salts than in the *N*-methylated salts (Table 1). The ESP values plotted on the Hirshfeld surface of cations are similar in 3-bromopyridinium cations while in case of 3-iodopyridinium cations *N*-methylated one have somewhat smaller ESP value than the *N*-ethylated one. All in all, there is no significant difference in halogen bonding between the *N*-ethylated and the *N*-methylated halogenopyridinium cations with iodide anions.

**Table 1.** An overview of the  $\text{C-X}\cdots\text{I}^-$  halogen bonds and ESP values in  $\sigma$ -hole area in the *N*-ethylated and *N*-methylated 3-halogenopyridines [104].

	<i>N</i> -ethylated			<i>N</i> -methylated		
	$d(\text{XB})/\text{\AA}$	<i>R.S.</i> (XB)/%	ESP (X)/ $\text{kJ mol}^{-1} \text{e}^{-1}$	$d(\text{XB})/\text{\AA}$	<i>R.S.</i> (XB)	ESP (X)/ $\text{kJ mol}^{-1} \text{e}^{-1}$
3ClPy	/	/	294	3.776	−1.2	381
3BrPy	3.611	5.7	449	3.637	5.0	452
3IPy	3.473	12.3	570	3.538	10.7	554

Interestingly, while the reaction of iodoethane with 3-chloropyridine and 3-iodopyridine in acetone yielded only the expected *N*-ethyl-3-pyridinium iodides, 3-bromopyridine yielded a mixture of the expected *[N*-Et-3-Brpy]I and *N*-(2-oxopropyl)-3-bromopyridinium iodide (*[N*-Ace-3Brpy]I, Figure 4a). This by-product was formed by reaction of an acetone molecule with 3-bromopyridine, presumably through the formation of an intermediate iodoacetone in situ. When dichloromethane was used as the solvent, only pure *[N*-Et-3-Brpy]I was obtained.

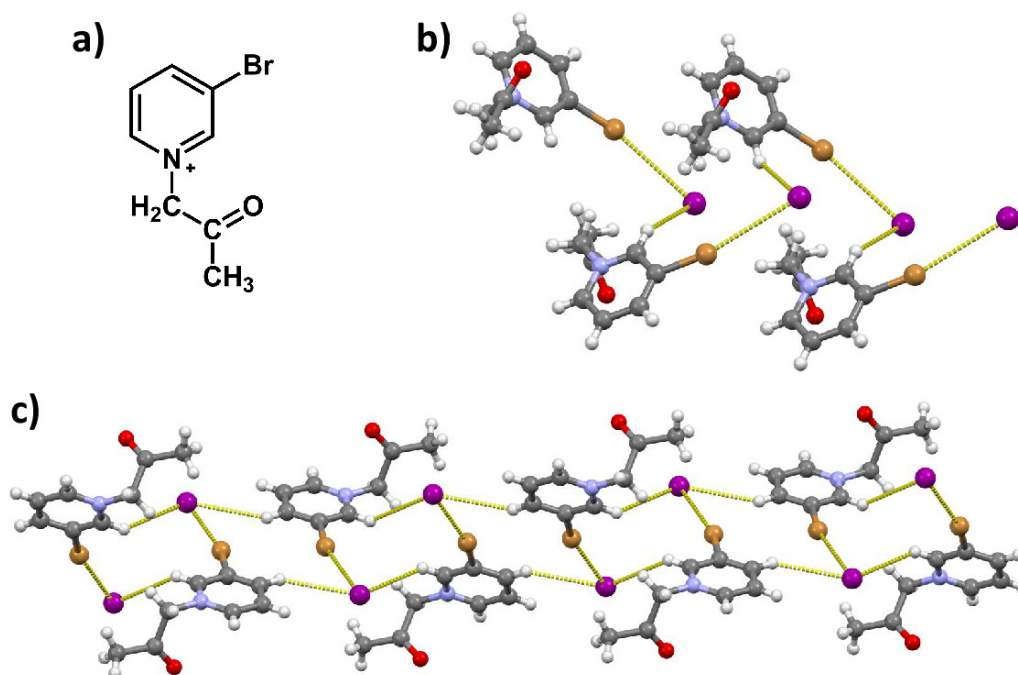


**Figure 4.** (a) *[N*-Ace-3-BrPy]<sup>+</sup> cation; (b) *[N*-Ace-3-BrPy]<sup>+</sup> cations and iodide anions connected through C–Br···I<sup>−</sup> halogen bonds and C–H···I<sup>−</sup> hydrogen bonds into chains in the structure of *[N*-Ace-3-BrPy]I; (c) View along crystallographic *b* axis—chains connected into layer through C–H···I<sup>−</sup> hydrogen bonds.

In the structure of *[N*-Ace-3-Brpy]I, the bromine atom again forms a halogen bond with the iodide anion ( $d(\text{Br}1 \cdots \text{I}1) = 3.694(7) \text{ \AA}$ ,  $\angle(\text{C}2-\text{Br}1 \cdots \text{I}1) = 166.4(1)^\circ$ ). Iodide anion also binds *[N*-Ace-3-Brpy]<sup>+</sup> cation through C–H···I<sup>−</sup> hydrogen bonds ( $d(\text{C}1 \cdots \text{I}1) = 3.754(4) \text{ \AA}$ ) with an aromatic hydrogen atom in *ortho* position to the pyridine nitrogen which lead to the formation of helical chains extending along the crystallographic *b* axis (Figure 4b). A different set of C–H···I<sup>−</sup> hydrogen bonds ( $d(\text{C}3 \cdots \text{I}1) = 3.847(5) \text{ \AA}$ ) leads to the formation of the 2D structure (Figure 4c).

In order to expand the series of *N*-ethylated iodopyridinium salts, we have attempted to synthesize *N*-ethyl-4-iodopyridinium iodide from 4-iodopyridine and ethyl iodide. However, despite numerous attempts of synthesis, we were not able to isolate the desired product. Instead, when the reaction was performed in a mixture of hot acetone and dichloromethane, a minute amount (two single crystals) of solid product was obtained, which was identified as 4-iodopyridinium hemihydroiodide ((4-IPy)<sub>2</sub>HI). It was presumably formed by a reaction of 4-IPy and the traces of hydroiodic acid produced by hydrolysis of ethyl iodide with water absorbed from the atmosphere over time. Although in the structure of (4-IPy)<sub>2</sub>HI the position of the HI hydrogen atom could not be ascertained from the electron difference map, it is evident that it is placed between the nitrogen atoms of a pair of molecules, interconnecting them by a charge assisted [119] (probably symmetrical) N···H···N hydrogen bond ( $d(\text{N} \cdots \text{N}) = 3.202(8) \text{ \AA}$ ) into a [(4-IPy)<sub>2</sub>H]<sup>+</sup> complex. The iodide anion participates in two C–I···I<sup>−</sup> halogen bonds ( $d(\text{I}1 \cdots \text{I}3) = 3.502(7) \text{ \AA}$ ,  $\angle(\text{C}3-\text{I}1 \cdots \text{I}3) = 173.8(2)^\circ$ ;  $d(\text{I}2 \cdots \text{I}3) = 3.533(7) \text{ \AA}$ ,  $\angle(\text{C}8-\text{I}2 \cdots \text{I}3) = 172.7(2)^\circ$ ), with two neighbouring [(4-IPy)<sub>2</sub>H]<sup>+</sup> hydrogen-bonded complexes. This combination of hydrogen

and halogen bonds forms supramolecular chains which are further connected into double chains through C–H···I<sup>−</sup> hydrogen bonds ( $d(\text{C6} \cdots \text{I1}) = 4.028(7) \text{ \AA}$ ) (Figure 5). It is interesting to note that this structure presents an excellent illustration of the HSAB principle in supramolecular chemistry[120,121]—the iodine atom of the  $[(4\text{-IPy})_2\text{H}]^+$  complex is the *softer* Lewis acid and therefore preferentially binds to the *softer* Lewis base, i.e., iodide. In contrast, the proton is the *hardest* Lewis acid and preferentially bind to the *harder* Lewis base, i.e., pyridine nitrogen.

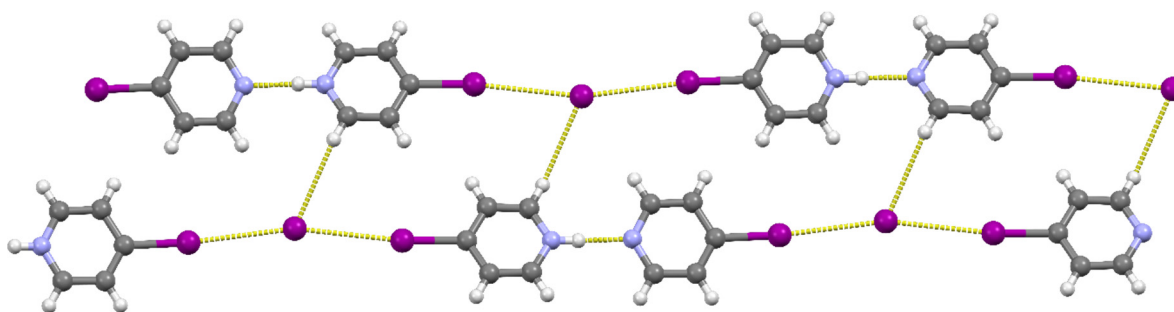


**Figure 5.**  $[(4\text{-IPy})_2\text{H}]^+$  hydrogen bonded complexes and iodide anions connected through C–I···I<sup>−</sup> halogen bonds and C–H···I<sup>−</sup> hydrogen bonds into double chains in the structure of  $[(4\text{-IPy})_2\text{H}]\text{I}$ .

As shown above, the hydrogen bonded  $[(4\text{-IPy})_2\text{H}]^+$  complex acts in the crystal structure of  $(4\text{-IPy})_2\text{HI}$  as a linear ditopic cationic halogen bond donor. This observation inspired us to attempt deliberate synthesis of ditopic cationic halogen bond donors by linking a pair of iodinated pyridine rings with different hydrocarbon linkers. For this purpose, we selected **3-IPy** (which has shown to be a more reliable substrate for *N*-alkylation) as the iodopyridine, and propylene and (*E*)-buta-2-enylene chains as linkers. These linkers were selected as the latter was expected to result in a linear ditopic donor (due to the constricted rotation about the double bond), while the former would result in a bent molecule (the linker being an odd-numbered hydrocarbon chain).

The reaction of **3-IPy** with 1,3-diiodopropane in 2:1 ratio, which was expected to produce the bent dication did not yield the desired product. Instead, we obtained *N*-(3-iodopropane)-3-iodopyridinium iodide ( $[N\text{-IProp-3-IPy}]\text{I}$ ).  $[N\text{-IProp-3-IPy}]\text{I}$  crystallized in centrosymmetric  $P2_1/c$  space group with two crystallographically independent ion pairs in the asymmetric unit. This structure comprised chains of alternating cations and anions connected by C–I···I<sup>−</sup> halogen bonds (Figure 6). In spite of the fact that only one iodine atom of the reactant 1,3-diiodopropane was substituted by **3-IPy**, the cations acted as ditopic halogen bond donors. Both cations bind two iodide anions, one through C–I···I<sup>−</sup> halogen bonds ( $d(\text{I1} \cdots \text{I5}) = 3.487(7) \text{ \AA}$ ,  $\angle(\text{C2-I1} \cdots \text{I5}) = 174.3(2)^\circ$ ;  $d(\text{I3} \cdots \text{I6}) = 3.558(7) \text{ \AA}$ ,  $\angle(\text{C10-I3} \cdots \text{I6}) = 174.4(2)^\circ$ ) with the iodine bonded to pyridine ring, and the other through C–I···I<sup>−</sup> halogen bonds ( $d(\text{I4} \cdots \text{I5}) = 3.870(8) \text{ \AA}$ ,  $\angle(\text{C8-I4} \cdots \text{I5}) = 176.0(2)^\circ$ ;  $d(\text{I2} \cdots \text{I6}) = 4.044(8) \text{ \AA}$ ,  $\angle(\text{C16-I2} \cdots \text{I6}) = 152.4(2)^\circ$ ) with the iodine atom bonded to alkyl chain. Halogen bonds involving the pyridine iodine atom as halogen bond donor are ca. 10% and 12% shorter than the sum of the corresponding van der Waals radii. On the other hand, one of the two halogen bonds involving an alkyl iodine atom as a halogen bond donor is ca. 2% shorter, while the other one is ca. 2% longer than the sum of the corresponding van der Waals radii. The neighbouring chains are further interconnected by a network of C–H···I<sup>−</sup> and C–H···I contacts in a 3D structure (Figure 6).

Unlike 1,3-diiodopropane, (*E*)-1,4-dibromobuta-2-ene reacted with **3-IPy** in the expected 1:2 ratio, yielding a bromide salt of a  $[N,N'\text{-Buen-(3-IPy)}_2]^{2+}$  cation (Figure 7a). This salt crystallized in the centrosymmetric space group  $P 2_1/c$  with the cation placed on an inversion centre. The cation binds two bromide anions via C–I···Br<sup>−</sup> halogen bonds ( $d(\text{I1} \cdots \text{Br1}) = 3.240(6) \text{ \AA}$ ,  $\angle(\text{C2-I1} \cdots \text{Br1}) = 174.5(1)^\circ$ ). In addition to this halogen bond, the bromide anion participates only in C–H···Br<sup>−</sup> hydrogen bonds with aromatic and

methine hydrogen atoms of four neighbouring cations (Figure 7b) leading to formation of a 3D structure.

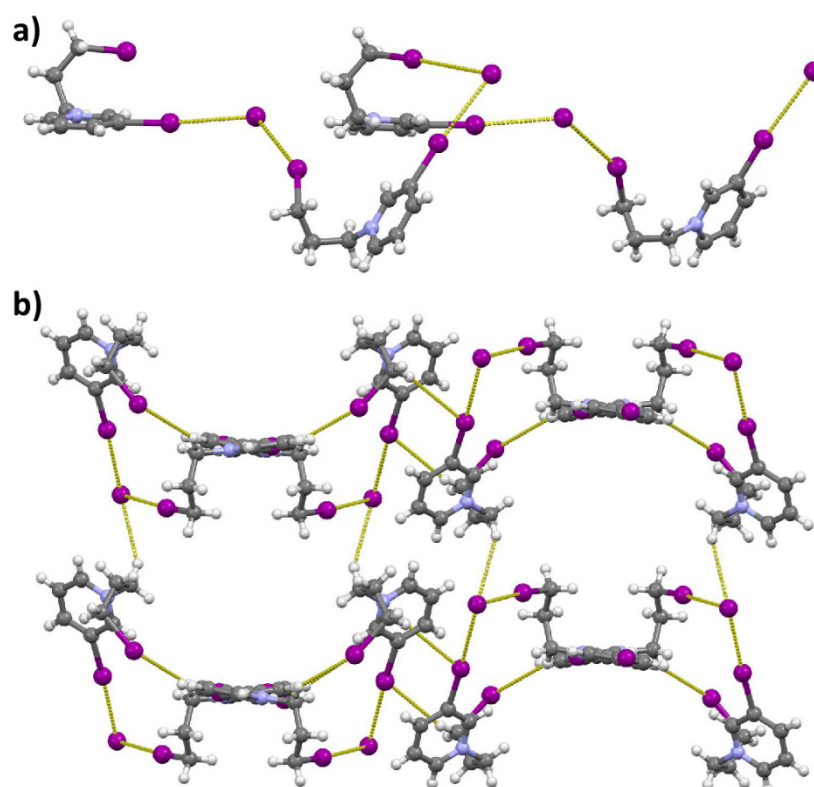


**Figure 6.** (a)  $[N\text{-IProp-3-IPy}]^+$  cations and iodide anions connected through  $\text{C-I}\cdots\text{I}^-$  halogen bonds in chains in the structure of  $[N\text{-Et-3-IPy}]\text{I}$ ; (b) Neighbouring chains are further interconnected by a network of  $\text{C-H}\cdots\text{I}^-$  and  $\text{C-H}\cdots\text{I}$  contacts into a 3D structure.

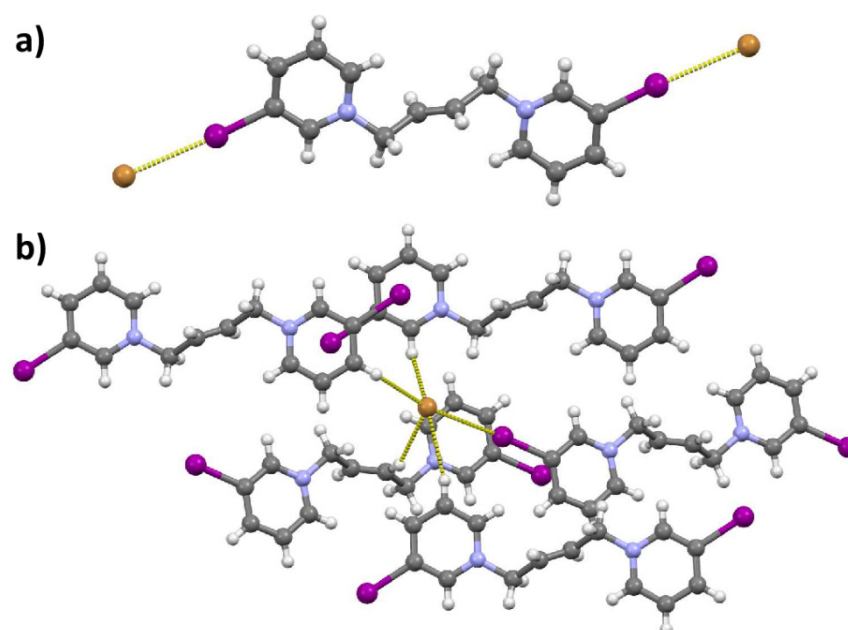


**Figure 7.** (a) One  $[N,N'\text{-Buen-(3-IPy)}_2]^{2+}$  cation binds two bromide anions by  $\text{C-I}\cdots\text{Br}^-$  halogen bonds in the structure of  $[N,N'\text{-Buen-(3-IPy)}_2]\text{Br}_2$ ; (b) Bromide anion binds four neighbouring cations through  $\text{C-H}\cdots\text{Br}^-$  and one cation through  $\text{C-I}\cdots\text{Br}^-$  halogen bonds leading to formation of a 3D structure.

In order to be able to better compare the  $[N,N'\text{-Buen-(3-IPy)}_2]^{2+}$  cation to other halogen bond donors covered by this study (all obtained as iodide salts), we attempted to obtain its iodide salt by ion exchange. Unfortunately, the cation was decomposed by the process: instead of the expected product, we obtained  $[N\text{-IBuen-(3-IPy)}]I$ , an iodide salt of a monocation equivalent to the  $[N\text{-IProp-3-IPy}]^+$  cation described above. In contrast to  $[N\text{-IProp-3-IPy}]I$ , in  $[N\text{-IBuen-(3-IPy)}]I$ , the cation does not act as a ditopic donor. Only the pyridyl iodine atoms participate in halogen bonding with iodide anions. The  $C-I\cdots I^-$  halogen bonds are ca. 14% and 10% shorter than the sum of the corresponding van der Waals radii ( $d(I1\cdots I3) = 3.395(1) \text{ \AA}$ ,  $\angle (C2-I1\cdots I5) = 176.1(4)^\circ$ ;  $d(I4\cdots I6) = 3.569(1) \text{ \AA}$ ,  $\angle (C11-I4\cdots I6) = 177.2(4)^\circ$ ). Those two halogen-bonded ion pairs (independent by symmetry) are connected in tetramers through  $C-H\cdots I^-$  hydrogen bonds with methylene and aromatic hydrogen atoms (*ortho* to the pyridine nitrogen) ( $d(C1\cdots I6) = 3.841(1) \text{ \AA}$ ,  $d(C6\cdots I6) = 3.874(2) \text{ \AA}$ ;  $d(C10\cdots I3) = 3.852(1) \text{ \AA}$ ,  $d(C15\cdots I3) = 3.987(1) \text{ \AA}$ ). Tetramers are linked into chains through  $C-H\cdots I^-$  hydrogen bonds with hydrogen atoms in *meta* position to the pyridine nitrogen atom ( $d(C4\cdots I6) = 3.961(2) \text{ \AA}$ ,  $d(C13\cdots I3) = 3.918(2) \text{ \AA}$ ) (Figure 8).

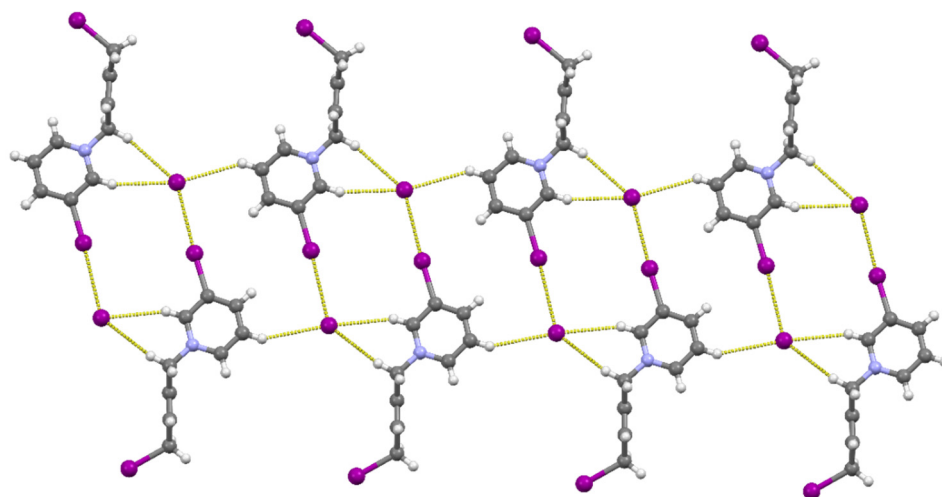


**Figure 8.**  $[N\text{-IBuen-(3-IPy)}]^+$  cations and iodide anions connected through  $C-I\cdots I^-$  halogen and  $C-H\cdots I^-$  hydrogen bonds in cyclical  $[N\text{-IBuen-(3-IPy)}]_2I_2$  tetramers linked via  $C-H\cdots I^-$  hydrogen bonds into chains the structure of  $[N\text{-IBuen-(3-IPy)}]I$ .

The failure of the alkyl iodine atom of  $[N\text{-IBuen-(3-IPy)}]^+$  to act as a donor of a halogen bond can be rationalised by an examination of the ESP values plotted on the Hirshfeld surfaces of the cations (Figure 9a). Generally, it can be seen that the positive charge is mainly located around pyridine nitrogen atom and neighbouring atoms (carbon and hydrogen) and spread on the pyridine ring rather than on the alkyl chain. As a result, the ESP in the region of the  $\sigma$ -hole of the aliphatic iodine atom on the aliphatic chain is considerably lower than that of the iodine on the pyridine ring. Consequently, the aliphatic iodine atom is a weaker halogen bond donor. This can also be seen from the comparison of the lengths of the  $C-I\cdots I^-$  halogen bond involving pyridine iodine atom and aliphatic iodine atom as halogen bond donor in  $[N\text{-IProp-3-IPy}]I$ . Halogen bonds involving iodine atoms bonded to pyridine ring (ESP of 0.227 a.u. and 0.203 a.u.) are ca. 10–14% shorter than the sum of the corresponding van der Waals radii, while those involving iodine bonded to the aliphatic chain are in one case (ESP of 0.118 a.u.) slightly shorter, and in the other (ESP of 0.100 a.u.) even longer, than the sum of the corresponding van der Waals radii (Figure 9a).

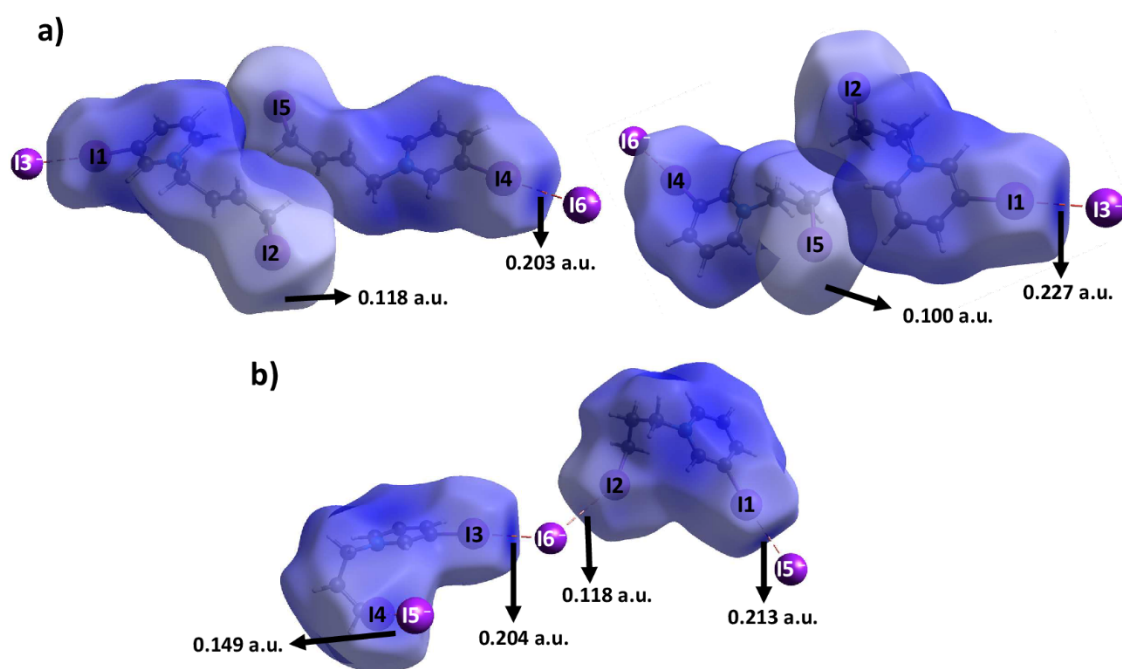


**Figure 9.** Hirshfeld surface with mapped ESP (computed on B3LYP-DGDZVP level of theory) for: (a)  $[N\text{-IBuen-(3-IPy)}]^+$  cation and (b)  $[N\text{-IProp-(3-IPy)}]^+$  cation.

If we compare the  $C_{\text{py}}-\text{I}\cdots\text{I}^-$  halogen bonds in  $[N\text{-IProp-3-IPy}]\text{I}$  and  $[N\text{-IBuen-(3-IPy)}]\text{I}$ , we can see that  $[N\text{-IBuen-(3-IPy)}]^+$  forms somewhat shorter halogen bond with iodide anion than  $[N\text{-IProp-(3-IPy)}]^+$  cation. Furthermore although the  $C_{\text{py}}-\text{I}\cdots\text{I}^-$  halogen bonds in  $[N\text{-IProp-3-IPy}]\text{I}$  are somewhat longer than the one in  $[N\text{-Et-3-IPy}]\text{I}$ , there appears to be a trend of longer chains as  $N$ -substituents generally leading to shorter  $C_{\text{py}}-\text{I}\cdots\text{I}^-$  halogen bonds in  $N$ -alkyl-3-iodopyridinium iodides (Figure 10a). The values of ESP corresponding to the  $\sigma$ -hole of the iodine on the pyridinium ring (plotted on the Hirshfeld surfaces of these four cations in the crystal structures of the corresponding iodides) also follow the same trend, with the  $\sigma$ -hole of the iodine being the most positive in  $[N\text{-IBuen-(3-IPy)}]^+$ , and least positive in  $[N\text{-Me-3-IPy}]^+$  (Figure 10b).

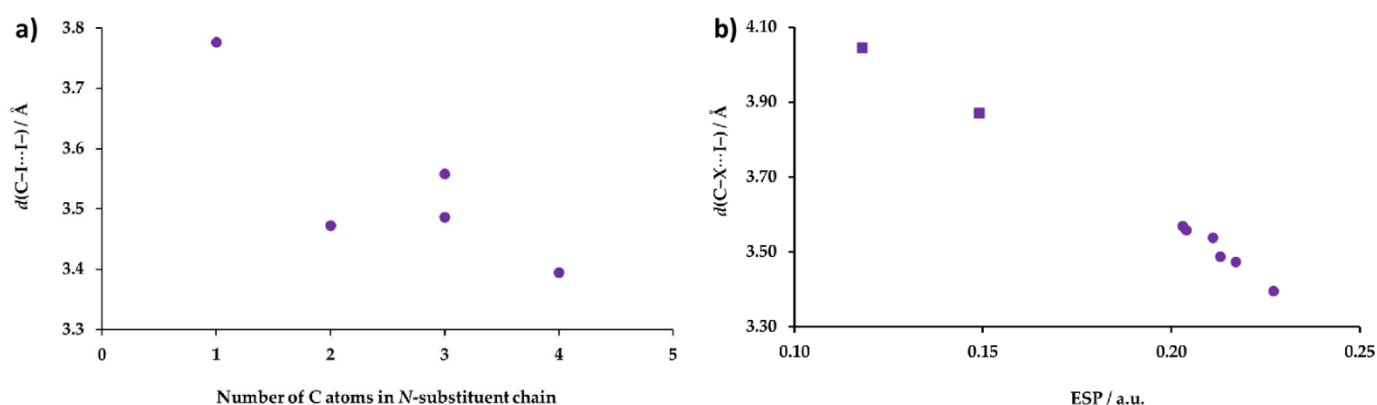


**Figure 10.** (a) Correlation of the number of carbon atoms in  $N$ -substituent chain of  $N$ -alkyl-3-iodopyridinium cations with  $\text{C-I}\cdots\text{I}^-$  halogen bonds lengths; (b) plot of the values of ESP corresponding to the  $\sigma$ -hole of the halogen atom. vs.  $\text{C-X}\cdots\text{I}^-$  halogen bonds lengths.

#### 4. Conclusions

Introducing various (aliphatic) *N*-substituents on the pyridine ring of 3-bromo- and 3-iodopyridine appears to be a viable method for preparation of an entire class of cationic halogen bond donors. Using aliphatic dihalogenides to produce bis-(halogenopyridinium) dications capable of acting as ditopic halogen bond donors has proven to be somewhat less successful—of the two attempted target cations, only one was isolated, and it decomposed during an attempted ion exchange. However, this opened the possibility of the synthesis of potentially ditopic asymmetric aliphatic–aromatic monocationic halogen bond donors, with two halogens which greatly differ in ESP values corresponding to the halogen  $\sigma$ -hole, and therefore in halogen bonding potential.

**Supplementary Materials:** The following are available online at <https://www.mdpi.com/article/10.3390/cryst11101240/s1>, Figure S1. Molecular structure of [N-Et-3-ClPy]I showing the atom-labelling scheme. Displacement ellipsoids are drawn at the 50% probability level, and H atoms are shown as small spheres of arbitrary radius; Figure S2. Molecular structure of [N-Et-3-BrPy]I showing the atom-labelling scheme. Displacement ellipsoids are drawn at the 50% probability level, and H atoms are shown as small spheres of arbitrary radius; Figure S3. Molecular structure of [N-Et-3-IPy]I showing the atom-labelling scheme. Displacement ellipsoids are drawn at the 50% probability level, and H atoms are shown as small spheres of arbitrary radius; Figure S4. Molecular structure of [N-Ace-3-ClPy]I showing the atom-labelling scheme. Displacement ellipsoids are drawn at the 50% probability level, and H atoms are shown as small spheres of arbitrary radius; Figure S5. Molecular structure of [4-IPy]<sub>2</sub>HI showing the atom-labelling scheme. Displacement ellipsoids are drawn at the 50% probability level, and H atoms are shown as small spheres of arbitrary radius; Figure S6. Molecular structure of [N-PropI-3-IPy]I showing the atom-labelling scheme. Displacement ellipsoids are drawn at the 50% probability level, and H atoms are shown as small spheres of arbitrary radius; Figure S7. Molecular structure of [N,N'-Buen-(3-IPy)<sub>2</sub>]Br<sub>2</sub> showing the atom-labelling scheme. Displacement ellipsoids are drawn at the 50% probability level, and H atoms are shown as small spheres of arbitrary radius; Figure S8. Molecular structure of [N-BuenI-3-IPy]I showing the atom-labelling scheme. Displacement ellipsoids are drawn at the 50% probability level, and H atoms are shown as small spheres of arbitrary radius; Figure S9. Measured (black) and calculated (blue) PXRD patterns of [N-Et-3-ClPy]I; Figure S10. Measured (black) and calculated (blue) PXRD patterns of [N-Et-3-BrPy]I; Figure S11. Measured (black) and calculated (blue) PXRD patterns of [N-Et-3-IPy]I; Figure S12. Measured (black) and calculated (blue) PXRD patterns of [N-PropI-3-IPy]Br; Figure S13. Measured (black) and calculated (blue) PXRD patterns of [N,N'-Buen-(3-IPy)<sub>2</sub>]Br<sub>2</sub>; Figure S14. Measured (black) and calculated (blue) PXRD patterns of [N-BuenI-3-IPy]I; Figure S15. TG (black) and DSC (red) thermograms of [N-Et-3-ClPy]I; Figure S16. TG (black) and DSC (red) thermograms of [N-Et-3-BrPy]I; Figure S17. TG (black) and DSC (red) thermograms of [N-Et-3-IPy]I; Figure S18. TG (black) and DSC (red) thermograms of [N-PropI-3-IPy]I; Figure S19. TG (black) and DSC (red) thermograms of [N,N'-Buen-(3-IPy)<sub>2</sub>]Br<sub>2</sub>; Figure S20. TG (black) and DSC (red) thermograms of [N-BuenI-3-IPy]I; Figure S21. IR spectrum (ATR) of [N-Et-3-ClPy]I; Figure S22. IR spectrum (ATR) of [N-Et-3-BrPy]I; Figure S23. IR spectrum (ATR) of [N-Et-3-IPy]I; Figure S24. IR spectrum (ATR) of [N-PropI-3-IPy]I; Figure S25. IR spectrum (ATR) of [N,N'-Buen-(3-IPy)<sub>2</sub>]Br<sub>2</sub>; Figure S26. IR spectrum (ATR) of [N-BuenI-3-IPy]I; Table S1. An overview and crystallographic data of the prepared compounds. CCDC 2109490–2109497 contain crystallographic data for this paper. These data can be obtained free of charge from the Director, CCDC, 12 Union Road, Cambridge, CBZ 1EZ, UK (Fax: +44-1223-336033; email: deposit@ccdc.cam.ac.uk or www: <http://www.ccdc.cam.ac.uk> accessed on 25 August 2021).

**Author Contributions:** Conceptualization, L.F. and V.S.; methodology, L.F. and V.S.; formal analysis, L.F.; investigation, L.F.; data curation, L.F.; writing—original draft preparation, L.F.; writing—review and editing, L.F. and V.S.; visualization, L.F. and V.S.; supervision, V.S. All authors have read and agreed to the published version of the manuscript.

**Funding:** This research was funded by the Croatian Science Foundation under the project IP-2019-04-1868.

**Institutional Review Board Statement:** Not applicable.

**Informed Consent Statement:** Not applicable.

**Data Availability Statement:** Not applicable.

**Acknowledgments:** We acknowledge the support of project CIuK co-financed by the Croatian Government and the European Union through the European Regional Development Fund-Competitiveness and Cohesion Operational Programme (Grant KK.01.1.1.02.0016.).

**Conflicts of Interest:** The authors declare no conflict of interest. The funders had no role in the design of the study; in the collection, analyses, or interpretation of data; in the writing of the manuscript, or in the decision to publish the results.

## References

1. Cavallo, G.; Metrangolo, P.; Milani, R.; Pilati, T.; Priimagi, A.; Resnati, G.; Terraneo, G. The halogen bond. *Chem. Rev.* **2016**, *116*, 2478–2601. [[CrossRef](#)]
2. Metrangolo, P.; Resnati, G. *Halogen Bonding*; Metrangolo, P., Resnati, G., Eds.; Springer: Berlin/Heidelberg, Germany, 2008; Volume 126.
3. Metrangolo, P.; Resnati, G. Halogen bonding: A paradigm in supramolecular chemistry. *Chem. Eur. J.* **2001**, *7*, 2511–2519. [[CrossRef](#)]
4. Erdélyi, M. Halogen bonding in solution. *Chem. Soc. Rev.* **2012**, *41*, 3547–3557. [[CrossRef](#)]
5. Gilday, L.C.; Robinson, S.W.; Barendt, T.A.; Langton, M.J.; Mullaney, B.R.; Beer, P.D. Halogen bonding in supramolecular chemistry. *Chem. Rev.* **2015**, *115*, 7118–7195. [[CrossRef](#)] [[PubMed](#)]
6. Politzer, P.; Murray, J.S.; Clark, T. Halogen bonding: An electrostatically-driven highly directional noncovalent interaction. *Phys. Chem. Chem. Phys.* **2010**, *12*, 7748–7757. [[CrossRef](#)] [[PubMed](#)]
7. Politzer, P.; Murray, J.S.; Clark, T.; Resnati, G. The  $\sigma$ -hole revisited. *Phys. Chem. Chem. Phys.* **2017**, *19*, 32166–32178. [[CrossRef](#)] [[PubMed](#)]
8. Legon, A.C. The halogen bond: An interim perspective. *Phys. Chem. Chem. Phys.* **2010**, *12*, 7736–7747. [[CrossRef](#)] [[PubMed](#)]
9. Cinčić, D.; Friščić, T.; Jones, W. Structural equivalence of Br and I halogen bonds: A route to isostructural materials with controllable properties. *Chem. Mater.* **2008**, *20*, 6623–6626. [[CrossRef](#)]
10. Ding, X.; Tuikka, M.; Haukk, M. Halogen Bonding in Crystal Engineering. In *Recent Advances in Crystallography*; InTech: London, UK, 2012; Volume 262, pp. 143–168.
11. Mukherjee, A.; Tothadi, S.; Desiraju, G.R. Halogen Bonds in Crystal Engineering: Like Hydrogen Bonds yet Different. *Acc. Chem. Res.* **2014**, *47*, 2514–2524. [[CrossRef](#)] [[PubMed](#)]
12. Aakeröy, C.B.; Wijethunga, T.K.; Desper, J. Practical crystal engineering using halogen bonding: A hierarchy based on calculated molecular electrostatic potential surfaces. *J. Mol. Struct.* **2014**, *1072*, 20–27. [[CrossRef](#)]
13. Bulfield, D.; Huber, S.M. Halogen Bonding in Organic Synthesis and Organocatalysis. *Chem. Eur. J.* **2016**, *22*, 14434–14450. [[CrossRef](#)]
14. Lisac, K.; Topić, F.; Arhangelskis, M.; Cepić, S.; Julien, P.A.; Nickels, C.W.; Morris, A.J.; Friščić, T.; Cinčić, D. Halogen-bonded cocrystallization with phosphorus, arsenic and antimony acceptors. *Nat. Commun.* **2019**, *10*, 61. [[CrossRef](#)]
15. Nemeč, V.; Lisac, K.; Bedeković, N.; Fotović, L.; Stilinović, V.; Cinčić, D. Crystal engineering strategies towards halogen-bonded metal-organic multi-component solids: Salts, cocrystals and salt cocrystals. *CrystEngComm* **2021**, *23*, 3063–3083. [[CrossRef](#)]
16. Aakeröy, C.B.; Baldrighi, M.; Desper, J.; Metrangolo, P.; Resnati, G. Supramolecular hierarchy among halogen-bond donors. *Chem. Eur. J.* **2013**, *19*, 16240–16247. [[CrossRef](#)] [[PubMed](#)]
17. Aakeröy, C.B.; Wijethunga, T.K.; Haj, M.A.; Desper, J.; Moore, C. The structural landscape of heteroaryl-2-imidazoles: Competing halogen-and hydrogen-bond interactions. *CrystEngComm* **2014**, *16*, 7218. [[CrossRef](#)]
18. Eraković, M.; Cinčić, D.; Molčanov, K.; Stilinović, V. A Crystallographic Charge Density Study of the Partial Covalent Nature of Strong N $\cdots$ Br Halogen Bonds. *Angew. Chem. Int. Ed.* **2019**, *58*, 15702–15706. [[CrossRef](#)]
19. Aakeröy, C.B.; Wijethunga, T.K.; Desper, J.; Đaković, M. Electrostatic Potential Differences and Halogen-Bond Selectivity. *Cryst. Growth Des.* **2016**, *16*, 2662–2670. [[CrossRef](#)]
20. Turunen, L.; Warzok, U.; Puttreddy, R.; Beyeh, N.K.; Schalley, C.A.; Rissanen, K. [N $\cdots$ I $^+\cdots$ N] Halogen-Bonded Dimeric Capsules from Tetrakis(3-pyridyl)ethylene Cavitations. *Angew. Chem. Int. Ed.* **2016**, *55*, 14033–14036. [[CrossRef](#)] [[PubMed](#)]
21. Turunen, L.; Pan, F.; Beyeh, N.K.; Trant, J.F.; Ras, R.H.A.; Rissanen, K. Bamboo-like Chained Cavities and Other Halogen-Bonded Complexes from Tetrahaloethynyl Cavitations with Simple Ditopic Halogen Bond Acceptors. *Cryst. Growth Des.* **2018**, *18*, 513–520. [[CrossRef](#)]
22. Saccone, M.; Siiskonen, A.; Fernandez-Palacio, F.; Priimagi, A.; Terraneo, G.; Resnati, G.; Metrangolo, P. Halogen bonding stabilizes a *cis*-azobenzene derivative in the solid state: A crystallographic study. *Acta Crystallogr. Sect. B Struct. Sci. Cryst. Eng. Mater.* **2017**, *73*, 227–233. [[CrossRef](#)]
23. Meazza, L.; Foster, J.A.; Fucke, K.; Metrangolo, P.; Resnati, G.; Steed, J.W. Halogen-bonding-triggered supramolecular gel formation. *Nat. Chem.* **2013**, *5*, 42–47. [[CrossRef](#)] [[PubMed](#)]
24. Saccone, M.; Cavallo, G.; Metrangolo, P.; Pace, A.; Pibiri, I.; Pilati, T.; Resnati, G.; Terraneo, G. Halogen bond directionality translates tecton geometry into self-assembled architecture geometry. *CrystEngComm* **2013**, *15*, 3102–3105. [[CrossRef](#)]

25. Jakupec, N.; Fotović, L.; Stilinović, V. The effect of halogen bonding on protonated hexacyanoferrate networks in hexacyanoferrates of halogenopyridines. *CrystEngComm* **2020**, *22*, 8142–8150. [[CrossRef](#)]
26. Uran, E.; Fotović, L.; Bedeković, N.; Stilinović, V.; Cinčić, D. The amine group as halogen bond acceptor in cocrystals of aromatic diamines and perfluorinated iodobenzenes. *Crystals* **2021**, *11*, 529. [[CrossRef](#)]
27. Aakeröy, C.B.; Wijethunga, T.K.; Benton, J.; Desper, J. Stabilizing volatile liquid chemicals using co-crystallization. *Chem. Commun.* **2015**, *51*, 2425–2428. [[CrossRef](#)]
28. Aakeröy, C.B.; Wijethunga, T.K.; Desper, J. Constructing molecular polygons using halogen bonding and bifurcated *N*-oxides. *CrystEngComm* **2014**, *16*, 28–31. [[CrossRef](#)]
29. Carletta, A.; Zbačnik, M.; Vitković, M.; Tumanov, N.; Stilinović, V.; Wouters, J.; Cinčić, D. Halogen-bonded cocrystals of *N*-salicylidene Schiff bases and iodoperfluorinated benzenes: Hydroxyl oxygen as a halogen bond acceptor. *CrystEngComm* **2018**, *20*, 5332–5339. [[CrossRef](#)]
30. Topić, F.; Lisac, K.; Arhangelskis, M.; Rissanen, K.; Cinčić, D.; Friščić, T. Cocrystal trimorphism as a consequence of the orthogonality of halogen- and hydrogen-bonds synthons. *Chem. Commun.* **2019**, *55*, 14066–14069. [[CrossRef](#)]
31. Martinez, V.; Bedeković, N.; Stilinović, V.; Cinčić, D. Tautomeric Equilibrium of an asymmetric  $\beta$ -diketone in halogen-bonded cocrystals with perfluorinated iodobenzenes. *Crystals* **2021**, *11*, 699. [[CrossRef](#)]
32. Stilinović, V.; Grgurić, T.; Piteša, T.; Nemeč, V.; Cinčić, D. Bifurcated and monocentric halogen bonds in cocrystals of metal(ii) acetylacetonates with *p*-dihalotetrafluorobenzenes. *Cryst. Growth Des.* **2019**, *19*, 1245–1256. [[CrossRef](#)]
33. Nemeč, V.; Piteša, T.; Friščić, T.; Cinčić, D. The morpholinyl oxygen atom as an acceptor site for halogen-bonded cocrystallization of organic and metal–organic units. *Cryst. Growth Des.* **2020**, *20*, 3617–3624. [[CrossRef](#)]
34. Syssa-Magalá, J.-L.; Boubekour, K.; Schöllhorn, B. First molecular self-assembly of 1,4-diiodo-tetrafluoro-benzene and a ketone via (O $\cdots$ I) non-covalent halogen bonds. *J. Mol. Struct.* **2005**, *737*, 103–107. [[CrossRef](#)]
35. Goodwin, M.J.; Steed, B.W.; Yufit, D.S.; Musa, O.M.; Berry, D.J.; Steed, J.W. Halogen and Hydrogen Bonding in Povidone-Iodine and Related Co-Phases. *Cryst. Growth Des.* **2017**, *17*, 5552–5558. [[CrossRef](#)]
36. Tothadi, S.; Sanphui, P.; Desiraju, G.R. Obtaining synthon modularity in ternary cocrystals with hydrogen bonds and halogen bonds. *Cryst. Growth Des.* **2014**, *14*, 5293–5302. [[CrossRef](#)]
37. Saha, B.K.; Nangia, A.; Jaskólski, M. Crystal engineering with hydrogen bonds and halogen bonds. *CrystEngComm* **2005**, *7*, 355. [[CrossRef](#)]
38. Cinčić, D.; Friščić, T. Synthesis of an extended halogen-bonded metal–organic structure in a one-pot mechanochemical reaction that combines covalent bonding, coordination chemistry and supramolecular synthesis. *CrystEngComm* **2014**, *16*, 10169–10172. [[CrossRef](#)]
39. Nemeč, V.; Fotović, L.; Vitasović, T.; Cinčić, D. Halogen bonding of the aldehyde oxygen atom in cocrystals of aromatic aldehydes and 1,4-diiodotetrafluorobenzene. *CrystEngComm* **2019**, *21*, 3251–3255. [[CrossRef](#)]
40. Nemeč, V.; Fotović, L.; Friščić, T.; Cinčić, D. A large family of halogen-bonded cocrystals involving metal-organic building blocks with open coordination sites. *Cryst. Growth Des.* **2017**, *17*, 6169–6173. [[CrossRef](#)]
41. Zbačnik, M.; Pajski, M.; Stilinović, V.; Vitković, M.; Cinčić, D. The halogen bonding proclivity of the: *Ortho*-methoxy-hydroxy group in cocrystals of *o*-vanillin imines and diiodotetrafluorobenzenes. *CrystEngComm* **2017**, *19*, 5576–5582. [[CrossRef](#)]
42. Lisac, K.; Cinčić, D. The Influence of Liquid on the Outcome of Halogen-Bonded Metal–Organic Materials Synthesis by Liquid Assisted Grinding. *Crystals* **2017**, *7*, 363. [[CrossRef](#)]
43. Lisac, K.; Cinčić, D. Simple design for metal-based halogen-bonded cocrystals utilizing the M–Cl $\cdots$ I motif. *CrystEngComm* **2018**, *20*, 5955–5963. [[CrossRef](#)]
44. Zordan, F.; Brammer, L. Water molecules insert into N–H $\cdots$ Cl–M hydrogen bonds while M–Cl $\cdots$ X–C halogen bonds remain intact in dihydrates of halopyridinium hexachloroplatinates. *Acta Crystallogr. Sect. B Struct. Sci.* **2004**, *60*, 512–519. [[CrossRef](#)] [[PubMed](#)]
45. Zordan, F.; Purver, S.L.; Adams, H.; Brammer, L. Halometallate and halide ions: Nucleophiles in competition for hydrogen bond and halogen bond formation in halopyridinium salts of mixed halide-halometallate anions. *CrystEngComm* **2005**, *7*, 350–354. [[CrossRef](#)]
46. Zordan, F.; Brammer, L.; Sherwood, P. Supramolecular chemistry of halogens: Complementary features of inorganic (M–X) and organic (C–X') halogens applied to M–X $\cdots$ X'–C halogen bond formation. *J. Am. Chem. Soc.* **2005**, *127*, 5979–5989. [[CrossRef](#)] [[PubMed](#)]
47. Decato, D.A.; Riel, A.M.S.; May, J.H.; Bryantsev, V.S.; Berryman, O.B. Theoretical, solid-state, and solution quantification of the hydrogen bond-enhanced halogen bond. *Angew. Chem.* **2021**, *133*, 3729–3736. [[CrossRef](#)]
48. Logothetis, T.A.; Meyer, F.; Metrangolo, P.; Pilati, T.; Resnati, G. Crystal engineering of brominated tectons: *N*-methyl-3,5-dibromopyridinium iodide gives particularly short C–Br $\cdots$ I halogen bonding. *New J. Chem.* **2004**, *28*, 760–763. [[CrossRef](#)]
49. Fotović, L.; Stilinović, V. Halogenide anions as halogen and hydrogen bond acceptors in iodopyridinium halogenides. *CrystEngComm* **2020**, *22*, 4039–4046. [[CrossRef](#)]
50. Awwadi, F.F.; Willett, R.D.; Peterson, K.A.; Twamley, B. The nature of halogen $\cdots$ halide synthons: Theoretical and crystallographic studies. *J. Phys. Chem. A.* **2007**, *111*, 2319–2328. [[CrossRef](#)]
51. Freytag, M.; Jones, P.G.; Ahrens, B.; Fischer, A.K. Hydrogen bonding and halogen-halogen interactions in 4-halopyridinium halides. *New J. Chem.* **1999**, *23*, 1137–1139. [[CrossRef](#)]

52. Willett, R.D.; Awwadi, F.; Butcher, R.; Haddad, S.; Twamley, B. The aryl bromine-halide ion synthon and its role in the control of the crystal structures of tetrahalocuprate (II) ions. *Cryst. Growth Des.* **2003**, *3*, 301–311. [CrossRef]
53. Brammer, L.; Mínguez Espallargas, G.; Adams, H. Involving metals in halogen-halogen interactions: Second-sphere Lewis acid ligands for perhalometallate ions (M-X···X'-C). *CrystEngComm* **2003**, *5*, 343–345. [CrossRef]
54. Mínguez Espallargas, G.; Brammer, L.; Sherwood, P. Designing intermolecular interactions between halogenated peripheries of inorganic and organic molecules: Electrostatically directed M-X···X'-C halogen bonds. *Angew. Chem. Int. Ed.* **2006**, *45*, 435–440. [CrossRef] [PubMed]
55. Roper, L.C.; Präsang, C.; Kozhevnikov, V.N.; Whitwood, A.C.; Karadakov, P.B.; Bruce, D.W. Experimental and theoretical study of halogen-bonded complexes of DMAP with di- and triiodofluorobenzenes. A complex with a very short N···I halogen bond. *Cryst. Growth Des.* **2010**, *10*, 3710–3720. [CrossRef]
56. Ding, X.H.; Chang, Y.Z.; Ou, C.J.; Lin, J.Y.; Xie, L.H.; Huang, W. Halogen bonding in the co-crystallization of potentially ditopic diiodotetrafluorobenzene: A powerful tool for constructing multicomponent supramolecular assemblies. *Natl. Sci. Rev.* **2020**, *7*, 1906–1932. [CrossRef]
57. Lunghi, A.; Cardillo, P.; Messina, T.; Metrangolo, P.; Panzeri, W.; Resnati, G. Perfluorocarbon-hydrocarbon self assembling. Thermal and vibrational analyses of one-dimensional networks formed by  $\alpha,\omega$ -diiodoperfluoroalkanes with K.2.2. and K.2.2.2. *J. Fluor. Chem.* **1998**, *91*, 191–194. [CrossRef]
58. Messina, M.T.; Metrangolo, P.; Panzeri, W.; Ragg, E.; Resnati, G. Perfluorocarbon-hydrocarbon self-assembly. Part 3. Liquid phase interactions between perfluoroalkylhalides and heteroatom containing hydrocarbons. *Tetrahedron Lett.* **1998**, *39*, 9069–9072. [CrossRef]
59. Farina, A.; Meille, S.V.; Messina, M.T.; Metrangolo, P.; Resnati, G.; Vecchio, G. Resolution of racemic 1,2-dibromohexafluoropropane through halogen-bonded supramolecular helices. *Angew. Chem. Int. Ed.* **1999**, *38*, 2433–2436. [CrossRef]
60. Metrangolo, P.; Meyer, F.; Pilati, T.; Resnati, G.; Terraneo, G. Halogen bonding in supramolecular chemistry. *Angew. Chem. —Int. Ed.* **2008**, *47*, 6114–6127. [CrossRef]
61. Raatikainen, K.; Rissanen, K. Hierarchical halogen bonding induces polymorphism. *CrystEngComm* **2009**, *11*, 750–752. [CrossRef]
62. Nguyen, S.T.; Ellington, T.L.; Allen, K.E.; Gorden, J.D.; Rheingold, A.L.; Tschumper, G.S.; Hammer, N.I.; Watkins, D.L. Systematic experimental and computational studies of substitution and hybridization effects in solid-state halogen bonded assemblies. *Cryst. Growth Des.* **2018**, *18*, 3244–3254. [CrossRef]
63. Rosokha, S.V.; Loboda, E.A. Interplay of halogen and  $\pi$ - $\pi$  charge-transfer bondings in intermolecular associates of bromo- or iododinitrobenzene with tetramethyl-*p*-phenylenediamine. *J. Phys. Chem. A.* **2015**, *119*, 3833–3842. [CrossRef]
64. Nwachukwu, C.I.; Kehoe, Z.R.; Bowling, N.P.; Speetzen, E.D.; Bosch, E. Cooperative halogen bonding and polarized  $\pi$ -stacking in the formation of coloured charge-transfer co-crystals. *New J. Chem.* **2018**, *42*, 10615–10622. [CrossRef]
65. Baykov, S.V.; Filimonov, S.I.; Rozhkov, A.V.; Novikov, A.S.; Ananyev, I.V.; Ivanov, D.M.; Kukushkin, V.Y. Reverse Sandwich structures from interplay between lone pair- $\pi$ -hole atom-directed C···dz<sup>2</sup>[M] and halogen bond interactions. *Cryst. Growth Des.* **2020**, *20*, 995–1008. [CrossRef]
66. Barry, D.E.; Hawes, C.S.; Blasco, S.; Gunnlaugsson, T. Structure Direction, solvent effects, and anion influences in halogen-bonded adducts of 2,6-bis(iodoethynyl)pyridine. *Cryst. Growth Des.* **2016**, *16*, 5194–5205. [CrossRef]
67. Nguyen, S.T.; Rheingold, A.L.; Tschumper, G.S.; Watkins, D.L. Elucidating the effects of fluoro and nitro substituents on halogen bond driven assemblies of pyridyl-capped  $\pi$ -conjugated molecules. *Cryst. Growth Des.* **2016**, *16*, 6648–6653. [CrossRef]
68. Baldrighi, M.; Bartesaghi, D.; Cavallo, G.; Chierotti, M.R.; Gobetto, R.; Metrangolo, P.; Pilati, T.; Resnati, G.; Terraneo, G. Polymorphs and co-crystals of haloprogin: An antifungal agent. *CrystEngComm* **2014**, *16*, 5897–5904. [CrossRef]
69. Stilinović, V.; Horvat, G.; Hrenar, T.; Nemeč, V.; Cinčić, D. Halogen and hydrogen bonding between (N-halogeno)-succinimides and pyridine derivatives in solution, the solid state and in silico. *Chem. Eur. J.* **2017**, *23*, 5244–5257. [CrossRef]
70. Raatikainen, K.; Rissanen, K. Interaction between amines and N-haloimides: A new motif for unprecedentedly short Br···N and I···N halogen bonds. *CrystEngComm* **2011**, *13*, 6972–6977. [CrossRef]
71. Raatikainen, K.; Rissanen, K. Breathing molecular crystals: Halogen- and hydrogen-bonded porous molecular crystals with solvent induced adaptation of the nanosized channels. *Chem. Sci.* **2012**, *3*, 1235–1239. [CrossRef]
72. Makhotkina, O.; Lieffrig, J.; Jeannin, O.; Fourmigué, M.; Aubert, E.; Espinosa, E. Cocrystal or salt: Solid state-controlled iodine shift in crystalline halogen-bonded systems. *Cryst. Growth Des.* **2015**, *15*, 3464–3473. [CrossRef]
73. Puttreddy, R.; Jurček, O.; Bhowmik, S.; Mäkelä, T.; Rissanen, K. Very strong <sup>-</sup>N-X<sup>+</sup>···<sup>-</sup>O-N<sup>+</sup> halogen bonds. *Chem. Commun.* **2016**, *52*, 2338–2341. [CrossRef]
74. Puttreddy, R.; Rautiainen, J.M.; Mäkelä, T.; Rissanen, K. Strong N-X···O-N halogen bonds: A comprehensive study on N-halosaccharin pyridine N-oxide complexes. *Angew. Chem. Int. Ed.* **2019**, *58*, 18610–18618. [CrossRef]
75. Mavračić, J.; Cinčić, D.; Kaitner, B. Halogen bonding of: N-bromosuccinimide by grinding. *CrystEngComm* **2016**, *18*, 3343–3346. [CrossRef]
76. Dolenc, D.; Modec, B. EDA Complexes of N-halosaccharins with N- and O-donor ligands. *New J. Chem.* **2009**, *33*, 2344–2349. [CrossRef]
77. Yu, S.; Ward, J.S.; Truong, K.; Rissanen, K. Carbonyl hypiodites as extremely strong halogen bond donors. *Angew. Chem. Int. Ed.* **2021**, *60*, 20739–20743. [CrossRef]

78. Aubert, E.; Espinosa, E.; Nicolas, I.; Jeannin, O.; Fourmigué, M. Toward a reverse hierarchy of halogen bonding between bromine and iodine. *Faraday Discuss.* **2017**, *203*, 389–406. [[CrossRef](#)]
79. Thomas, L.H.; Adam, M.S.; O'Neill, A.; Wilson, C.C. Utilizing proton transfer to produce molecular salts in bromanilic acid substituted-pyridine molecular complexes-predictable synthons? *Acta Crystallogr. Sect. C Cryst. Struct. Commun.* **2013**, *69*, 1279–1288. [[CrossRef](#)]
80. Espallargas, G.M.; Zordan, F.; Marín, L.A.; Adams, H.; Shankland, K.; van de Streek, J.; Brammer, L. Rational modification of the hierarchy of intermolecular interactions in molecular crystal structures by using tunable halogen Bonds. *Chem. Eur. J.* **2009**, *15*, 7554–7568. [[CrossRef](#)] [[PubMed](#)]
81. Awwadi, F.F.; Willett, R.D.; Twamley, B. The aryl chlorine-halide ion synthon and its role in the control of the crystal structures of tetrahalocuprate(II) ions. *Cryst. Growth Des.* **2007**, *7*, 624–632. [[CrossRef](#)]
82. Vitorica-Yrezabal, I.J.; Sullivan, R.A.; Purver, S.L.; Curfs, C.; Tang, C.C.; Brammer, L. Synthesis and polymorphism of (4-ClpyH)<sub>2</sub>[CuCl<sub>4</sub>]: Solid-gas and solid-solid reactions. *CrystEngComm* **2011**, *13*, 3189–3196. [[CrossRef](#)]
83. Wolf, J.; Huber, F.; Erochok, N.; Heinen, F.; Guérin, V.; Legault, C.Y.; Kirsch, S.F.; Huber, S.M. Activation of a metal-halogen bond by halogen bonding. *Angew. Chem. Int. Ed.* **2020**, *59*, 16496–16500. [[CrossRef](#)]
84. Sutar, R.L.; Engelage, E.; Stoll, R.; Huber, S.M. Bidentate chiral bis(imidazolium)-based halogen-bond donors: Synthesis and applications in enantioselective recognition and catalysis. *Angew. Chem. Int. Ed.* **2020**, *59*, 6806–6810. [[CrossRef](#)]
85. Derossi, S.; Brammer, L.; Hunter, C.A.; Ward, M.D. Halogen bonded supramolecular assemblies of [Ru(bipy)(CN)<sub>4</sub>]<sup>2-</sup> anions and *N*-methyl-halopyridinium cations in the solid state and in solution. *Inorg. Chem.* **2009**, *48*, 1666–1677. [[CrossRef](#)] [[PubMed](#)]
86. Ormond-Prout, J.E.; Smart, P.; Brammer, L. Cyanometallates as halogen bond acceptors. *Cryst. Growth Des.* **2012**, *12*, 205–216. [[CrossRef](#)]
87. Awwadi, F.F.; Willett, R.D.; Twamley, B. The Role of Charge Assisted Arylhalogen-Halide Ion Interactions in the Structures of the Dibromopyridinium Halide Salts. *J. Mol. Struct.* **2009**, *918*, 116–122. [[CrossRef](#)]
88. Awwadi, F.F.; Taher, D.; Kailani, M.H.; Alwahsh, M.I.; Odeh, F.; Rüffer, T.; Schaarschmidt, D.; Lang, H. Halogen Bonding Interactions in Halopyridine–Iodine Monochloride Complexes. *Cryst. Growth Des.* **2020**, *20*, 543–551. [[CrossRef](#)]
89. Awwadi, F.F.; Taher, D.; Maabreh, A.; Alwedian, F.Z.; Al-Ebaisat, H.; Rüffer, T.; Lang, H. The Role of Fe–X···X–Fe Contacts in the Crystal Structures of [(2-Iodopyridinium)<sub>2</sub>FeX<sub>4</sub>]X (X = Cl, Br). *Struct. Chem.* **2013**, *24*, 401–408. [[CrossRef](#)]
90. Bondarenko, M.A.; Adonin, S.A.; Novikov, A.S.; Sokolov, M.N.; Fedin, V.P. Supramolecular Bromoantimonate(V) Polybromide (2,6-BrPyH)<sub>3</sub>[SbBr<sub>6</sub>]{(Br<sub>2</sub>)Br} · 2H<sub>2</sub>O: Specific Features of Halogen···Halogen Contacts in the Crystal Structure. *Russ. J. Coord. Chem.* **2020**, *46*, 302–307. [[CrossRef](#)]
91. Anagnostis, J.; Cipi, J.; Landee, C.P.; Tremelling, G.W.; Turnbull, M.M.; Twamley, B.; Wikaira, J.L. Transition Metal Salts of 2-Amino-3,5-Dihalopyridine—Dimers: Syntheses, Structures and Magnetic Properties of (3,5-DiCAPH)<sub>2</sub>Cu<sub>2</sub>Br<sub>6</sub> and (3,5-DiBAPH)<sub>2</sub>Cu<sub>2</sub> × 6. *J. Coord. Chem.* **2017**, *70*, 3892–3906. [[CrossRef](#)]
92. Amendola, V.; Bergamaschi, G.; Boiocchi, M.; Fusco, N.; La Rocca, M.V.; Linati, L.; Lo Presti, E.; Mella, M.; Metrangolo, P.; Miljkovic, A. Novel hydrogen- and halogen-bonding anion receptors based on 3-iodopyridinium units. *RSC Adv.* **2016**, *6*, 67540–67549. [[CrossRef](#)]
93. Riel, A.M.S.; Jessop, M.J.; Decato, D.A.; Massena, C.J.; Nascimento, V.R.; Berryman, O.B. Experimental investigation of halogen-bond hard-soft acid-base complementarity. *Acta Crystallogr. Sect. B Struct. Sci. Cryst. Eng. Mater.* **2017**, *73*, 203–209. [[CrossRef](#)] [[PubMed](#)]
94. Riel, A.M.S.; Decato, D.A.; Sun, J.; Massena, C.J.; Jessop, M.J.; Berryman, O.B. The intramolecular hydrogen bonded-halogen bond: A new strategy for preorganization and enhanced binding. *Chem. Sci.* **2018**, *9*, 5828–5836. [[CrossRef](#)] [[PubMed](#)]
95. Foyle, É.M.; White, N.G. Anion templated crystal engineering of halogen bonding tripodal tris(halopyridinium) compounds. *CrystEngComm* **2020**, *22*, 2526–2536. [[CrossRef](#)]
96. Lohrman, J.A.; Deng, C.L.; Shear, T.A.; Zakharov, L.N.; Haley, M.M.; Johnson, D.W. Methanesulfonyl-polarized halogen bonding enables strong halide recognition in an arylethynyl anion receptor. *Chem. Commun.* **2019**, *55*, 1919–1922. [[CrossRef](#)]
97. Jungbauer, S.H.; Huber, S.M. Cationic multidentate halogen-bond donors in halide abstraction organocatalysis: Catalyst optimization by preorganization. *J. Am. Chem. Soc.* **2015**, *137*, 12110–12120. [[CrossRef](#)]
98. Adonin, S.A.; Gorokh, I.D.; Novikov, A.S.; Samsonenko, D.G.; Yushina, I.V.; Sokolov, M.N.; Fedin, V.P. Halobismuthates with Halopyridinium Cations: Appearance or Non-Appearance of Unusual Colouring. *CrystEngComm* **2018**, *20*, 7766–7772. [[CrossRef](#)]
99. Adonin, S.A.; Gorokh, I.D.; Novikov, A.S.; Abramov, P.A.; Sokolov, M.N.; Fedin, V.P. Halogen Contacts-Induced Unusual Coloring in Bi III Bromide Complex: Anion-to-Cation Charge Transfer via Br···Br Interactions. *Chem. A Eur. J.* **2017**, *23*, 15612–15616. [[CrossRef](#)]
100. Kosaka, Y.; Yamamoto, H.M.; Nakao, A.; Tamura, M.; Kato, R. Coexistence of conducting and magnetic electrons based on molecular  $\pi$ -electrons in the supramolecular conductor (Me-3,5-DIP)[Ni(dmit)<sub>2</sub>]<sub>2</sub>. *J. Am. Chem. Soc.* **2007**, *129*, 3054–3055. [[CrossRef](#)]
101. Kusamoto, T.; Yamamoto, H.M.; Tajima, N.; Oshima, Y.; Yamashita, S.; Kato, R. Bilayer mott system based on Ni(dmit)<sub>2</sub> (dmit = 1,3-dithiole-2-thione-4,5-dithiolate) anion radicals: Two isostructural salts exhibit contrasting magnetic behavior. *Inorg. Chem.* **2012**, *51*, 11645–11654. [[CrossRef](#)]

102. Kosaka, Y.; Yamamoto, H.M.; Tajima, A.; Nakao, A.; Cui, H.; Kato, R. Supramolecular Ni(dmit)<sub>2</sub> salts with halopyridinium cations—development of multifunctional molecular conductors with the use of competing supramolecular interactions. *CrystEngComm* **2013**, *15*, 3200–3211. [CrossRef]
103. Ren, X.; Meng, Q.; Song, Y.; Lu, C.; Hu, C.; Chen, X. Unusual magnetic properties of one-dimensional molecule-based magnets associated with a structural phase transition. *Inorg. Chem.* **2002**, *41*, 5686–5692. [CrossRef] [PubMed]
104. Fotović, L.; Stilinović, V. Evaluation of halogenopyridinium cations as halogen bond donors. *Cryst. Growth Des.* Unpublished work.
105. Degen, T.; Sadki, M.; Bron, E.; König, U.; Nénert, G. The HighScore suite. *Powder Diffr.* **2014**, *29*, S13–S18. [CrossRef]
106. CrysAlis PRO CCD. *User Inspired Software for Single Crystal X-ray Diffractometers*; Rigaku Corporation: Tokyo, Japan, 2014.
107. Manual, U. CrysAlis Pro. Power. 2010. Available online: [https://www.agilent.com/cs/library/usermanuals/Public/CrysAlis\\_Pro\\_User\\_Manual.pdf](https://www.agilent.com/cs/library/usermanuals/Public/CrysAlis_Pro_User_Manual.pdf) (accessed on 17 July 2021).
108. Sheldrick, G.M. SHELXT—Integrated space-group and crystal-structure determination. *Acta Crystallogr. Sect. A Found. Crystallogr.* **2015**, *71*, 3–8. [CrossRef] [PubMed]
109. Sheldrick, G.M. Crystal structure refinement with SHELXL. *Acta Crystallogr. Sect. C Struct. Chem.* **2015**, *71*, 3–8. [CrossRef]
110. Farrugia, L.J. WinGX suite for small-molecule single-crystal crystallography. *J. Appl. Crystallogr.* **1999**, *32*, 837–838. [CrossRef]
111. Dolomanov, O.V.; Bourhis, L.J.; Gildea, R.J.; Howard, J.A.K.; Puschmann, H. OLEX2: A complete structure solution, refinement and analysis program. *J. Appl. Crystallogr.* **2009**, *42*, 339–341. [CrossRef]
112. Macrae, C.F.; Bruno, I.J.; Chisholm, J.A.; Edgington, P.R.; McCabe, P.; Pidcock, E.; Rodriguez-Monge, L.; Taylor, R.; van De Streek, J.; Wood, P.A. Mercury CSD 2.0—New features for the visualization and investigation of crystal structures. *J. Appl. Crystallogr.* **2008**, *41*, 466–470. [CrossRef]
113. STARe Software, v.15.00. *Thermal Analysis Software*; Mettler Toledo: Greifensee, Switzerland, 2016.
114. Spackman, P.R.; Turner, M.J.; McKinnon, J.J.; Wolff, S.K.; Grimwood, D.J.; Jayatilaka, D.; Spackman, M.A. CrystalExplorer: A program for Hirshfeld surface analysis, visualization and quantitative analysis of molecular crystals. *J. Appl. Crystallogr.* **2021**, *54*, 1006–1011. [CrossRef]
115. Lee, C.; Yang, W.; Parr, R.G. Development of the Colle-Salvetti correlation-energy formula into a functional of the electron density. *Phys. Rev. B.* **1988**, *37*, 785–789. [CrossRef]
116. Peverati, R.; Truhlar, D.G. An improved and broadly accurate local approximation to the exchange–correlation density functional: The MN12-L functional for electronic structure calculations in chemistry and physics. *Phys. Chem. Chem. Phys.* **2012**, *14*, 13171. [CrossRef] [PubMed]
117. Yurieva, A.G.; Poleshchuk, O.K.; Filimonov, V.D. Comparative analysis of a full-electron basis set and pseudopotential for the iodine atom in DFT quantum-chemical calculations of iodine-containing compounds. *J. Struct. Chem.* **2008**, *49*, 548–552. [CrossRef]
118. Feller, D. The role of databases in support of computational chemistry calculations. *J. Comput. Chem.* **1996**, *17*, 1571–1586. [CrossRef]
119. Gilli, G.; Gilli, P. Towards an unified hydrogen-bond theory. *J. Mol. Struct.* **2000**, *552*, S0022–S2860. [CrossRef]
120. Parr, R.G.; Chattaraj, P.K. Principle of maximum hardness. *J. Am. Chem. Soc.* **1991**, *113*, 1854–1855. [CrossRef]
121. Chattaraj, P.K.; Lee, H.; Parr, R.G. HSAB principle. *J. Am. Chem. Soc.* **1991**, *113*, 1855–1856. [CrossRef]